UNIVERSITÀ
DEGLI STUDI
DI TRIESTE

Thermal gelation modeling of a pluronic-alginate blend following coronary angioplasty

This is the peer reviewed (post-print) version of the following article:

Original
Thermal gelation modeling of a pluronic-alginate blend following coronary angioplasty / Milocco, A., Scuor, N., Lughi, V., Lamberti, G., Barba, A.A., Divittorio, R., Grassi, G., Perkan, A., Grassi, M., Abrami, M.. - In: JOURNAL OF APPLIED POLYMER SCIENCE. - ISSN 0021-8995. - STAMPA. - 137:25(2020), pp. 48539.1-48539.10. [10.1002/app.48539]

Availability:
This version is available at: 11368/2961686 since: 2020-04-09T10:55:17Z
Publisher:

Published
DOI:10.1002/app.48539
Terms of use:

Some rights reserved. More details in the PostPrint rights section below.

License:
Copyright Editore

Publisher copyright

-.-

(Article begins on next page)

06 October 2026

arTs Università degli Studi di Trieste
Archivio della ricerca – postprint

Thermal gelation modeling of a pluronic-alginate blend following coronary angioplasty

Alessio Milocco,[1] Nicola Scuor,[1] Vanni Lughi,[1] Gaetano Lamberti,[2] Anna Angela Barba,[3] Rosario Divittorio,[1] Gabriele Grassi,[4] Andrea Perkan,[5] Mario Grassi ,[1] Michela Abrami[1]

[1]Department of Engineering and Architecture, Trieste University, via Valerio 6, I-34127 Trieste, Italy
[2]Department of Industrial Engineering, University of Salerno, Via Giovanni Paolo II, 132, I-84084 Fisciano, SA, Italy
[3]Department of Pharmacy, Salerno University, Via Giovanni Paolo II, 132, I-84084 Fisciano, SA, Italy
[4]Department of Life Sciences, Cattinara University Hospital, Trieste University, Strada di Fiume 447, I-34149 Trieste, Italy
[5]Struttura Complessa di Cardiologia, Azienda per l'Assistenza Sanitaria n. 1 Triestina, Cattinara Hospital, Strada di Fiume 447, I-34149 Trieste, Italy
Correspondence to: M. Grassi (E-mail: mario.grassi@dia.units.it)

ABSTRACT: To overcome the complications connected to the treatment of coronary atherosclerosis by means of percutaneous transluminal angioplasty followed by stent implantation, the *in situ* release of antiproliferative nucleic acid based drugs (NABD) seems a promising approach. For their fragile nature, NABD cannot be released from drug eluting stents but they need to be embedded in a soft gel coating the coronary wall (endoluminal gel paving). This article deals with the thermal fate, once in the catheter, of a polymer blend composed by pluronic, giving rise to a soft gel in water upon temperature rise, and alginate, a natural polysaccharide giving origin to a strong gel in the presence of divalent cations. Simulations reveal that while the formation of a pregel is rapidly achieved, the formation of a mature gel takes a much longer time with respect to the residence time of the polymer blend inside the catheter. © 2019 Wiley Periodicals, Inc. J. Appl. Polym. Sci. **2020**, *137*, 48539.

DOI: 10.1002/app.48539

INTRODUCTION

Traditionally, coronary stenosis, a common atherosclerosis complication, has been treated by means of percutaneous transluminal coronary angioplasty (PTCA), a maneuver leading to the enlargement of the coronary stenotic portion by means of an expanding balloon. However, in about 30–50% of treated patients,[1] PTCA has been shown to induce the development of symptomatic re-occlusion (restenosis) caused by early elastic recoil, intimal hyperplasia (exuberant proliferation of vascular smooth muscle cells, VSMCs), late constricting remodeling of the vessel, and formation of mural thrombus.[2] Accordingly, alternative approaches were undertaken and the use of bare-metal stents (BMSs), rigid scaffolds located in correspondence of the coronary vessel stenotic portion, emerged as an interesting therapeutic strategy due to the significant reduction (down to 20–30% of the treated patients) of restenosis occurrence with respect to the simple PTCA treatment.[3–5] While BMSs could really prevent the coronary wall early elastic recoil and late remodeling, they could not solve the problem of neointima hyperplasia (In Stent Restenosis—ISR) due to the VSMCs hyperproliferation.[1,6] It was proposed that VSMCs switch from the contractile to the synthetic phenotype[7] plays a key role in triggering VSMC proliferative capacity. In addition, the increased number of VSMCs also depends on the movement of progenitor cells from the bone marrow to the injured vessel area.[8] Finally, macrophages, able to differentiate into myofibroblasts, also contribute to the hypercellularity.[9] VSMCs proliferation, although slowing down in time, persists months after stent implantation and is accompanied by an increased production of the extracellular matrix. The appearance of ISR was the reason why BMSs were substituted by first generation drug eluting stents (DESs), scaffolds designed for the localized delivery of antiproliferative drugs using stent walls (naked or covered by thin layers of degradable polymer) as the loading site. While first generation DESs did reduce ISR down to about 10% of the treated cases,[10] they were responsible for the increased incidence of in-stent thrombosis (IST)[11] probably due to an incomplete endothelialization of the stented zone in comparison with uncoated stents.[12] Indeed, it became evident that the antiproliferative and pro-apoptotic actions of the FDA-approved[13] antiproliferative drugs, Sirolimus (immune-suppressor of T-lymphocytes capable of reducing the inflammatory response, of down modulating VSMCs proliferation and promoting VSMCs apoptosis[14]) and Paclitaxel (microtubule stabilizing agent which reduces the concentration of free tubulin required for new tubulin formation.

This in turn down regulates biological processes such as cell proliferation and migration[15]), displayed side effects. In particular, they negatively regulate the growth of vascular endothelial cells, mainly responsible for the prevention of platelet adhesion and, thus, thrombus formation. The delayed re-endothelialization of the stented region is thought to significantly contribute to thrombus formation and, thus, to vessel restenosis.[16,17] This drawback induced to skip to second generation DES that were characterized by lower rates of IST but suffered by another complication leading to late or very late stent failure, known as neoatherosclerosis (NA),[18,19] which develops inside the stented segment of a coronary vessel.[20] NA probably develops in three distinct phases comprehending early infiltration by foamy macrophages, in-stent atherosclerotic plaque development, and formation of necrotic core plaque with a thin fibrous cap.[21] Interestingly, NA occurs more frequently in DESs than in BMS.[22] Consequently, the last 10 years saw the growth of the third generation DESs, implants that have undergone substantial structural improvements, such as thinner metallic struts and more biocompatible durable or biodegradable polymers.[23] However, despite the huge improvements of third generation DESs, the risks of NA and late stent failure are still present. Thus, authoritative authors believe that in the next future cardiovascular science will be focused on novel stent systems and antiproliferative drugs.[24] In particular, it seems that nucleic acid drugs (NABDs)[16,25,26] could play a very important role in this frame as they demonstrated a great therapeutic potential in many experimental models of intima hyperplasia.[24] However, their practical use demands for optimal delivery systems as, in the naked form, they are rapidly degraded in the cellular and extracellular fluids and they show a scarce cellular transfection attitude. A common solution to these drawbacks is represented by their complexation with proper delivery agents (DA) such as liposomes and polycations. The dimensions and the physicochemical characteristics of NABD–DA complexes make their release from DES problematic so that other solutions have to be considered. The endoluminal gel paving technique (EGP),[27] together with the use of a BMS, could be an effective and promising approach.[28] EGP consists of the catheter application of a biocompatible polymer solution on the endoluminal vessel surface followed by *in situ* polymerization or crosslinking. The potential benefits of EGP-BMS are an easy and safe complex loading within the polymer solution and the opportunity of creating a physical barrier between the damaged coronary wall and the overflowing thrombogenic and inflammatory elements present in the blood stream.[29] Furthermore, the presence of the physical barrier prevents from the effects connected to hemodynamic alterations (wall shear stress and local hemodynamic forces) that, after stent implantation, play an important role in restenosis, thrombosis, platelet activation, and NA.[24] Finally, considering a proper polymeric blend,[30–34] it is possible the realization of a double layers gel. While the strong part, in direct contact with blood flow, prevents from premature gel erosion and limits NABD–DA complexes systemic release, the soft part, comprised between coronary wall and the strong part, allows NABD–DA complexes delivery to the coronary wall where VSMCs reside. In particular, here the attention is focused on the thermal behavior of an aqueous solution hosting pluronic 127 (PF127),[35] a synthetic poly(oxyethylene–oxypropylene-oxyethylene) triblock copolymer undergoing thermal gelation in water, and alginate, an anionic linear natural polysaccharide extracted from brown seaweeds able to give origin to a strong physical gel in the presence of divalent cations.[36,37]

In particular, PF127 aqueous solutions show a non-Newtonian shear-thinning behavior[30] characterized by a huge difference (from three up to seven orders of magnitude depending on PF127 concentration and temperature) between the viscosity at zero shear and at very high shear. In addition, rheological oscillatory tests (stress and frequency sweep tests) reveal the typical gel behavior [storage (G') and loss (G'') moduli almost pulsation independent with $G' >> G''$] on condition that PF127 concentration and temperature are sufficiently high. The complexity of the PF127 rheological behavior can be explained by the different nanostructures it can form (cubic, hexagonal, lamellae) and by the flow-induced transitions from one structure to another one.[38,39]

The initial thermal gelation of PF127, induced by body temperature, serves to form the soft layer in contact with the coronary wall while the subsequent alginate ionotropic gelation yields to the strong layer facing the blood flow. To optimize the deposition of the polymeric blend solution on the coronary wall, it is of paramount importance to study the thermal gelation process that, theoretically, can start as soon as the solution is inserted in the catheter. Indeed, we would like that the polymeric solution can properly flow inside the catheter and form a gel once in contact with the coronary wall. The thermal fate of our polymeric solution was matched building up a proper mathematical model enabling the determination of the time evolution of the temperature profile in the solution while it moves inside the catheter. The kinetic of the sol–gel transition was studied by means of a rheological characterization.

Our simulations prove that, relaying on the set polymer concentration inside solution, a sort of pregel rapidly takes place inside the catheter while the formation of a true mature gel would require a much longer time with respect to the residence time of the polymeric system inside the catheter. In pregel condition, the system can adhere to the coronary wall embedding the stent strut and forming the right substrate for the formation of stronger gel due to the ionotropic gelation of alginate.

EXPERIMENTAL

Materials

Alginates are constituted by β-D-mannuronic (M) and a-L-guluronic (G) acid linked 1 → 4. The higher the G content, the stiffer and more fragile the gel they form in water in the presence of divalent cations. The alginate used in this article (molecular weight ≈10^6 Da), kind gift from FMC Biopolymer Ltd., UK, was characterized by a high G content (≈70% G and 30% M). Pluronic F127 (PF127) was purchased from Sigma-Aldrich Chemie GmbH, Germany.

Gel Preparation

The polymeric blend was prepared using the so-called "cold method" proposed by Schmolka.[40] A proper amount of alginate powder was slowly added to stirred distilled water contained in a beaker maintained at 7 °C. Subsequently, the desired amounts of Pluronic flakes were slowly added to the alginate solution. The system was stirred until complete polymer dissolution and then

kept at 4 °C for 12 h before use. The final alginate and pluronic mass fraction in the gel was, respectively, equal to 0.03 and 0.17 so that the "solid" mass fraction was equal to 0.2. Previous works of our group[30–34] suggested this composition.

Rheological Characterization

Rheological measurements were performed by a stress-controlled rotational rheometer (Haake Mars Rheometer, 379-0200 Thermo Electron GmbH, Karlsruhe, Germany) equipped by parallel plate geometry (PP35, ϕ = 35 mm, serrated surfaces to avoid slippage at the wall) with a gap of 2 mm. The measuring device was kept inside a glass bell under saturated humidity conditions to avoid evaporation effects. To simulate the gelation kinetics inside the catheter, time-sweep tests (1 Hz and 1 Pa) were performed setting different heating speeds (instantaneous, 0.27, 0.1, and 0.027 °C s^{-1}). To evaluate the gel properties under equilibrium conditions, one sample was let 4 h at 37 °C and then it was characterized by a stress sweep test (1 Hz) to assess the wideness of the linear viscoelastic region. Then, a frequency sweep test, performed inside the linear viscoelastic region (τ = 1 Pa), allowed the determination of systems mechanical spectra [elastic (G') and viscous (G'') moduli dependence on the solicitation frequency pulsation $\omega = 2\pi f$, f = solicitation frequency].

Differential Scanning Calorimetry

DSC characterization was performed by a heat flux NETZSCH DSC 200F3 (Gerätebau GmbH, Germany) to evaluate the specific heat at constant pressure C_p of our polymeric solution in the range 2–40 °C. Once uploaded in the crucible, the sample (≈31 mg) was let at 2 °C for 15 min for equilibration and, then, the heating ramp (1 °C min^{-1}) followed under Argon flux.

MATHEMATICAL MODEL

The Frame

To put the balloon and the stent in correspondence of the coronary stenosis, it is necessary inserting a needle in the femoral or radial artery of the patient after local anesthesia. If originally, the election choice was the femoral route, nowadays the miniaturization of stents, balloons, and catheters made the radial route much more desirable. The main advantage of this approach consists in the more superficial position of the radial artery with respect to the femoral one, making complications less frequent and simpler to manage. In addition, while patient compliance is considerably increased, hospitalization time is reduced. Of course, the main drawbacks of the radial route consist in small vessel calibers, possible spasm, and possible severe vessel tortuosity.[41,42] After needle puncturing, a wire is passed into the vessel *via* the needle up to the stenosis. Then, the needle is replaced by a sheath (bearing a hemostatic valve) sliding over the wire and making the access to the vessel easier.

The administration of an anticoagulant precedes the insertion of a catheter, equipped by the expanding balloon and the BMS, up to the stenosis. The correct positioning of the balloon is driven by a fluoroscope that can realize radiographic images thanks to the injection of a contrast fluid as depicted in Figure 1(a,b).

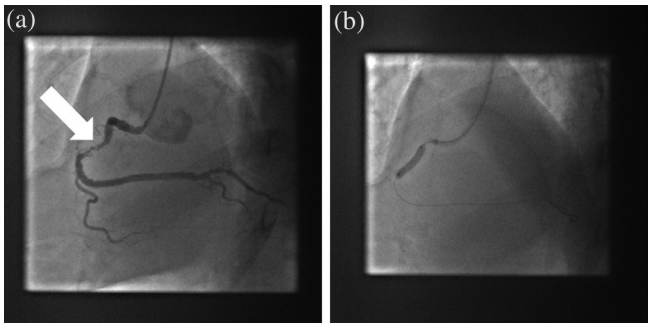

Figure 1. (a) The white arrow indicates the position of the coronary tight stenosis. (b) Inflated balloon with stent inside the stenosis. This picture has been provided by the "Struttura Complessa di Cardiologia, Azienda per l'Assistenza Sanitaria n. 1 Triestina, Cattinara Hospital, Strada di Fiume 447, I-34149 Trieste, Italy."

Modeling

As depicted in Figure 2(a–d), we propose that the deposition of the BMS and the gel on the coronary wall implies a series of different steps and two inflatable balloons. Once balloon 2 (that carrying the stent) has been positioned in the stenotic tract by the aid of a fluoroscope, as discussed in the previous section, balloon 1 is inflated to stop blood flow inside the vessel. Then, balloon 2 is expanded to enlarge the stenotic portion pushing the stent strut and the aqueous polymeric blend against the coronary wall. Thanks to body temperature, PF127 thermal gelation occurs (this approach is widely used in animal models[43–45]), so that a weak physical gel, embedding the stent strut, is formed on the coronary wall. After balloon 2 collapse, the release of a divalent cations solution from the catheter induces the ionotropic gelation of alginate that forms a strong physical gel aimed to resist to the eroding action exerted by blood flow. Cation solution is let in contact with the gel for a fixed time (contact time), elapsed which balloon 1 is collapsed and the normal blood flow is restored. According to this procedure, an inhomogeneous gel formed by a soft part, due to PF127 thermal gelation and adherent to the coronary wall, and a strong one, due to the ionotropic gelation of alginate and facing the blood flow, is formed. Indeed, while the PF127 thermal gelation involves the entire solution volume, this does not happen for the alginate ionotropic gelation due to both the thickness of the gel layer adhering to the coronary wall and the limited capacity of the divalent cations to pervade this thickness during the contact time.

If, on the one hand, a thick gel layer is desirable to guarantee a better and prolonged shielding action, a higher drug dose and a prolonged release, on the other hand a too thick gel causes an unacceptable pressure drop across the stented zone. For this purpose, Grassi *et al.*[46] estimated that, assuming a coronary diameter of about 3 mm, gel thickness should not exceed about 300 μm. In addition, Barba *et al.*[47] demonstrated that, assuming a real value of the contact time (≤2 min), cations penetration depth is lower than about 200 μm, whatever cations concentration (in the range 1–5 g L^{-1}) and alginate guluronic content (in the range 70–40%) are.

To guarantee a correct and uniform deposition on the coronary wall, and to limit the flow resistance, the polymeric blend must behave as a solution inside the catheter, while it is demanded to

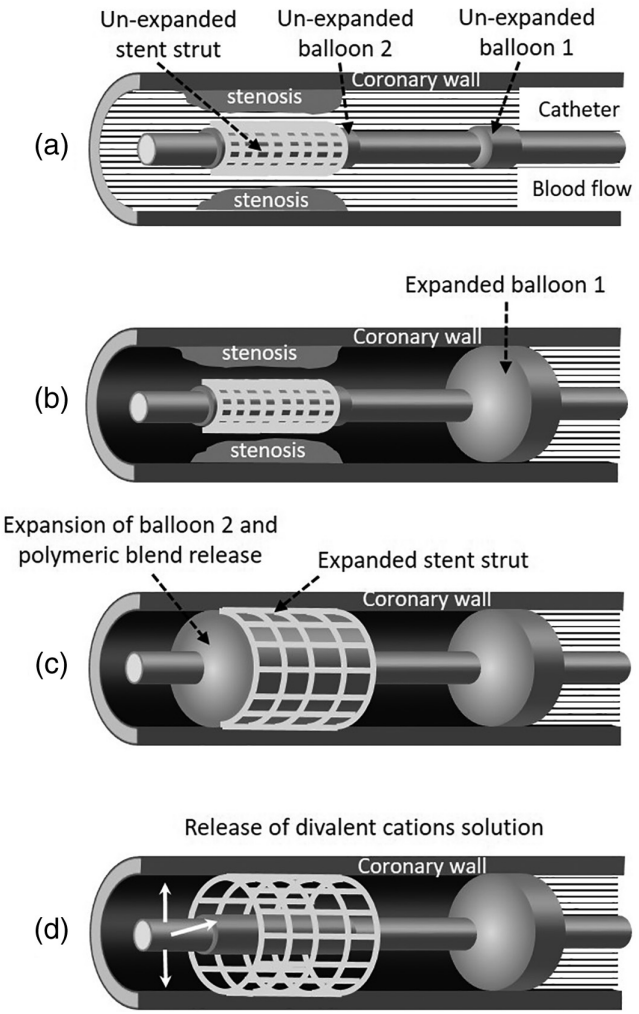

Figure 2. (a) The unexpanded balloon carrying the un-expanded stent strut is brought inside the stenotic zone. (b) Balloon 1 is inflated to hinder blood flow. (c) Balloon 2 is inflated to enlarge the stenosis, to expand the stent strut and to release the aqueous polymeric blend. (d) After balloon 2 collapse, the release of a divalent cations solution enables the ionotropic gelation of alginate (see white arrows).

immediately undergo gelation once in contact with the coronary wall. Thus, the attention must be focused on the relation between the heating of the polymer blend solution and its thermal transition toward a gel state. To simulate solution heating, we assume that the movement of the polymeric blend solution inside the catheter occurs according to a plug flow mechanism, that is, the velocity profile is flat whatever the radial position. Indeed, this seems the most reasonable assumption to adopt to study the flow of a small solution volume (≈30 mm^3) inside the catheter. Thus, the problem reduces to study the thermal heating of a known volume of polymeric blend solution in contact with catheter wall for the time required to push the solution up to the stenosis (≈120 s). In addition, although this is, intrinsically, a three-dimensional problem in cylindrical coordinates, we can suppose that the tangential temperature gradient is zero for symmetry reasons, while the axial one is negligible in comparison to the radial one. Indeed, relaying on the dimension of the catheter and the solution volume to be injected, the surface normal to the radial direction is about 10 times the surface normal to the axial direction. In these hypotheses, the energy balance necessary to evaluate the heating of the flowing solution volume is given by:

$$\rho C_p \frac{\partial T}{\partial t} = \frac{1}{\mathrm{r}} \frac{\partial}{\partial r}\left(rk \frac{\partial T}{\partial r} \right) + \dot{\mathrm{q}}, \tag{1}$$

where ρ is the density, C_p is the specific heat at constant pressure, T is the temperature, r is the radial coordinate, k is the thermal conductivity, and $\dot{q}$ is the heat, per unit length, due to the solution friction with the catheter wall.

Equation (1) was solved assuming that the initial solution temperature was equal to 5 °C and that $\dot{q}$ is negligible due to a very low value ($\approx 10^{-3}$) of the Brinkman number. To properly set the boundary conditions and to be as close as possible to a real setup of the double balloons apparatus, we considered four different scenarios, of increasing complexity, depicted in Figure 3(a–d). In the first configuration [Figure 3(a)], the presence of the wire is neglected so that only two phases appear: the polymeric blend one (inner gray zone) and the catheter wall (outer dashed zone). We suppose that the radial component of the temperature gradient (the only one existing in our hypotheses) is zero on the catheter symmetry axis and that the temperature of the catheter wall equals body temperature (37 °C). The second scenario [Figure 3 (b)] represents an improvement of the first one as it accounts also for the presence of the metallic wire (dashed inner zone) on the catheter symmetry axis. Also in this case, a vanishing radial component of the temperature gradient on the wire symmetry axis is assumed and body temperature (37 °C) is set for what concerns the catheter wall and the wire. The third scenario [Figure 3 (c)] supposes that balloon 2 (dotted zone) is twisted around the metallic wire so that the polymeric blend occupies an annular region delimited by the catheter (outer dashed zone) and balloon 2. Due to its very small thickness, wire presence, from the thermal point of view, is neglected. In this configuration, the adhesion of the polymer blend to balloon 2 is ensured by shellac, a natural glue secreted by the female lac bug (Laccifer lacca). As in the previous case, the catheter wall temperature is set to 37 °C and the radial component of the temperature gradient is set to zero on the catheter axis. In contrast, the temperature of balloon 2 is set to 5 °C. Finally, the fourth scenario [Figure 3(d)] can be considered a development of the third one as, now, we assume that balloon 2 is hollow so that it can host the polymer blend (gray zone). In this configuration, polymer blend release to the stenotic zone occurs through small holes present on the balloon 2 external layer.[48] For the sake of simplicity and for their similar thermal properties, the catheter wall and the balloon2 external part are considered as just one phase characterized by balloon 2 thermal properties. In this case, we assume that the polymeric blend and balloon 2 are, initially, at 5 °C while the external part of the catheter-balloon 2 layer is set to 37 °C. Again, the radial component of the temperature gradient zeroes on the axial symmetry axis.

To get the time evolution of the temperature profile, eq. (1) was discretized on the different phases (polymer blend, catheter, wire or balloon 2) according to the control volume method.[49] The computational domain was subdivided in a one-dimensional grid

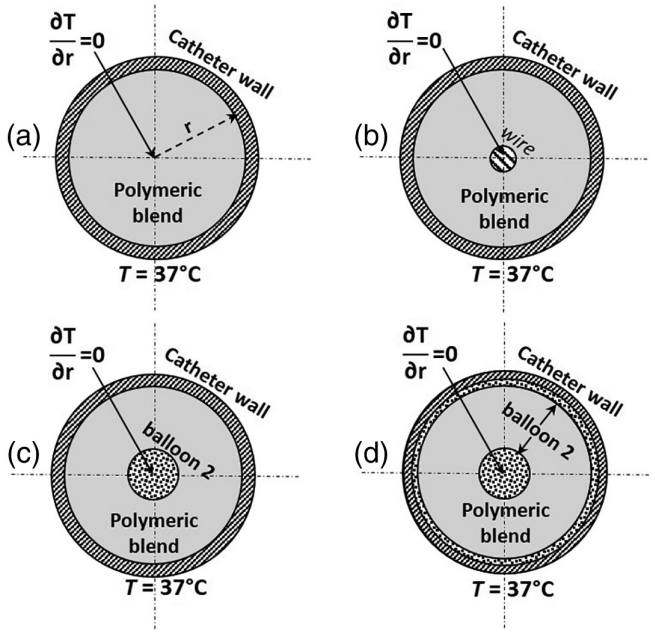

Figure 3. Cross-section of the four situations modeled (r indicates the radial coordinate). (a) Catheter lumen is completely filled by the polymer blend. (b) The presence of the wire laying on the symmetry axis of the catheter is considered. (c) Balloon 2 is symmetrically twisted on the wire. (d) Polymer blend is contained inside a hollow balloon 2.

constituted by 100 parts (grid dots were proportional the thickness of each phase) adopting 10^{-2} s as the time step. The resulting nonlinear system of equations was iteratively solved (relative tolerance 10^{-7}) through Gauss–Seidel's method.[50] The geometrical and thermal properties of wire (usually constituted by Nitinol, a nickel-titanium alloy), catheter (usually made up by nylon), and balloon 2 (usually realized by polyethylene terephthalate) are reported in Table I.

RESULTS AND DISCUSSION

DSC Characterization

Figure 4 shows the experimental trend of C_p (thick line) versus temperature for our polymer blend in the temperature range 5–40 °C. It is clear that C_p depends on temperature even if its variation is not so high. Interestingly, the peak appearing around 15 °C represents micellization, an endothermic phenomenon consisting in the aggregation of PF127 single chains (unimers) to form micelles, structures characterized by a central core built up of PPO hydrophobic segments and an external corona built up of PEO hydrophilic segments.[52]

In contrast, gelation, consisting in both micelle growth and aggregation, is a poorly endothermic transition that cannot be detected by means of DSC.[52] For what concerns the specific enthalpy of micellization, we found ≈4000 J kg^{-1}. This value and the peak temperature differ a little bit from that measured in Ref. 52 but alginate was not present in that case. To embody the C_p temperature dependence in our model [eq. (1)], the experimental data were fitted by the following empirical function (thin line in Figure 4):

$$C_p(T) = 0.3 + 4075e^{0.0038T^{1.2}} + 4701\left(\frac{2\times 5.78}{27.2}\right)\left(\frac{T-2}{27.2/2}\right)^{(5.78-1)} e^{\left(-\left(\frac{T-2}{27.2/2}\right)\right)^{(5.78-1)}} \quad (2)$$

Although not perfect, the experimental description of data provided by eq. (2) reasonably well defines the phenomenon.

Gelation and Heating Speed

One crucial aspect connected with the polymer blend transport inside the catheter and its deposition in the stenotic zone is the thermal gelation of PF127. In particular, we need to consider the effect of the heating speed as it is well known that this design parameter plays a very important role in the gelation process.[52] At this purpose, temperature sweep tests were performed at different heating speed as depicted in Figure 5. While 0.27 °C s^{-1} corresponds to a solution heating from 5 to 37 °C in about 120 s (i.e., the time the polymer blend resides inside the catheter), the other two serve to understand which are the effects of slower heating speeds. Figure 5 clearly shows that, whatever the heating speed, after an initial small reduction of G' and G'', an abrupt increase of both moduli takes place at a temperature depending on the heating speed. In particular, looking at the G' trend, we can see that the higher the heating speed, the higher the temperature of the abrupt increase. In addition, we can also see that the final G' value, that is, that at 37 °C, decreases with the heating speed. In particular, we can see that the final G' value corresponding to a heating speed of 0.27 °C s^{-1} is about one

Table I. Thermal and Geometrical Properties of Wire, Catheter, and Balloon 2[a]

Wire	Catheter	Balloon 2
ρ_w (kg m^{-3}) = 6500	ρ_c (kg m^{-3}) = 1130	ρ_b (kg m^{-3}) = 1380
C_{pw} (J kg^{-1} K^{-1}) = 450	C_{pc} (J kg^{-1} K^{-1}) = 1700	C_{pb} (J kg^{-1} K^{-1}) = 1050
k_w (W m^{-1} K^{-1}) = 18	k_c (W m^{-1} K^{-1}) = 0.25	k_b (W m^{-1} K^{-1}) = 0.28
ϕ_w (m) = 3.6 × 10^{-4}	ϕ_{int} (m) = 2 × 10^{-3}	ϕ_{sh} (m) = 4 × 10^{-4}
	ϕ_{ext} (m) = 2.1 × 10^{-3}	s_b (m) = 1 × 10^{-4}

ρ, C_p, and k indicate, respectively, density, specific heat at constant pressure, and thermal conductivity. ϕ_w is wire diameter, ϕ_{int}, and ϕ_{ext} are, respectively, catheter internal and external diameter, ϕ_{sb} is the diameter of balloon 2 in the shrunken state twisted on the wire [Figure 3(c,d)] and S_b indicates the thickness of the material constituting balloon 2.
[a] Data from Ref. 51.

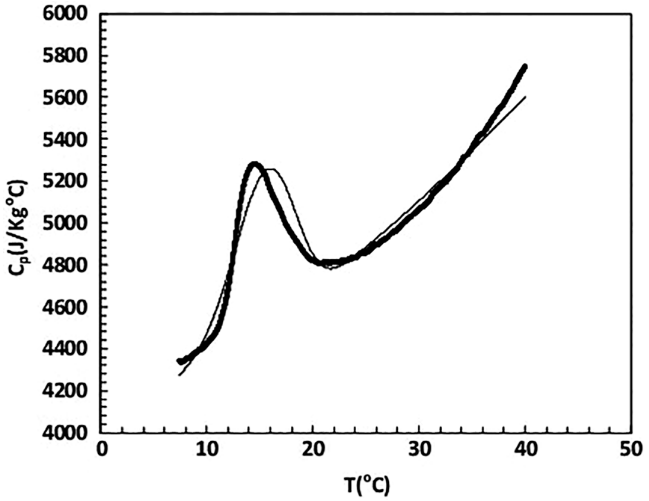

Figure 4. Comparison between the experimental trend (thick line) of the specific heat at constant pressure (C_p) and the best fitting (thin line) of the empirical eq. (2).

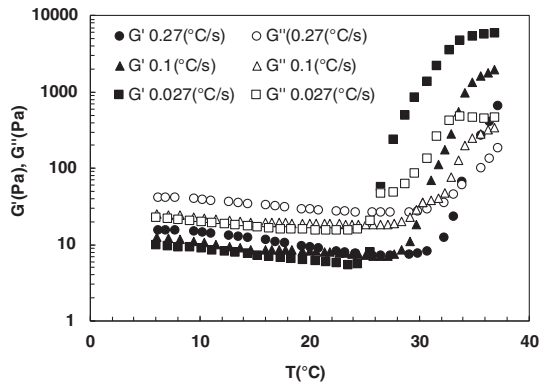

Figure 5. Effect of heating speed on the temperature (T) dependence of G', elastic modulus (filled symbols), and G'', viscous modulus (open symbols).

order of magnitude lower than that corresponding to a heating speed of 0.027 °C s^{-1}.

Although the definition of gel point would require a more sophisticated approach,[53] we can roughly assume that the sol–gel transition occurs when $tg\delta = G''/G' = 1$, δ being the dephase angle. More properly, we could refer to this situation as to the condition of an incipient or pregel status. According to this choice, the gelation temperature, T_{GEL}, turns out to be approximately proportional ($r^2 = 0.95$) to the heating speed (T_{GEL} = 26.6, 30.3, and 34 °C for heating speed of 0.027, 0.1, and 0.27 °C s^{-1}). Thus, heating speed increase not only reflects on a delayed beginning of gelation, but, more importantly, it reflects on smaller final G' (and G'') values. In other words, the increase of the heating speed pushes toward higher and higher temperature the entire gelation process and not only its beginning, as also found in Ref. 52. From the thermodynamic point of view, we could say that only when the heating speed is around 0.027 a real equilibrium condition is met.

Thus, it is clear that the heating speed reflects in different organizations of the PF127 nanostructure, this being potentially very important for the delivery of NABD. However, in this regard, we believe that the most important role is played by the superficial alginate crosslinking that gives origin to a strong network able to disrupt PF127 nanostructure into subdomains that are caged inside the alginate network.[32] Accordingly, due to the big dimension of naked or complexed NABDs, this layer can be considered impermeable to NABD. In contrast, NABD release toward the coronary wall could be affected by the PF127 nanostructure as, close to the coronary wall, alginate crosslinking does not take place due to the layer thickness and the limited diffusivity of divalent cations in it.

Interestingly, Figure 6 shows that, whatever the heating speed, after the abrupt increase, G', approximately, follows the time increase corresponding to the infinite heating speed. This means that the final G' value, corresponding to an equilibrium condition, will be reached in a time interval that is inversely proportional to the heating speed. Figure 7 clearly shows that the final values of G' and G'' reported in Figures 5 and 6 (for an infinite heating speed) equal those recorded in a frequency sweep test performed on a system in equilibrium condition. The correct comparison of moduli has to be performed at ω = 6.28 rad s^{-1}, as this was the pulsation used in the time sweep test of Figures 5 and 6. In addition, Figure 7 reveals that, in equilibrium

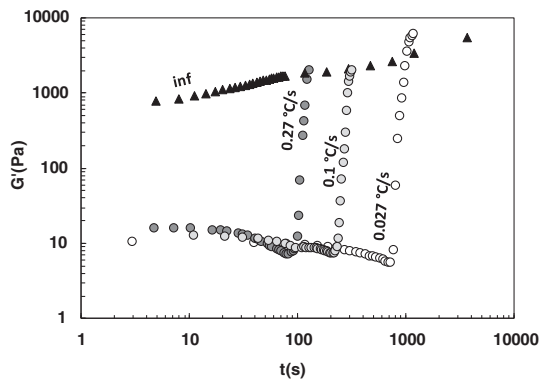

Figure 6. Temporal evolution of the storage modulus G' considering different heating speed. Open circles (0.027 °C s^{-1}), light gray circles (0.1 °C s^{-1}), dark gray circles (0.27 °C s^{-1}), and black triangles (instantaneous heating).

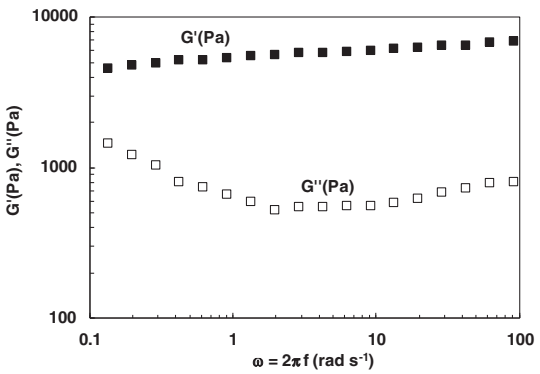

Figure 7. Mechanical spectra (frequency sweep test) referring to the polymer blend that underwent sol gel transition at a vanishing heating speed. ω is pulsation (=2$\pi \times f$, f = solicitation frequency), while G' and G'' are, respectively, the elastic (filled symbols) and viscous (open symbols) moduli.

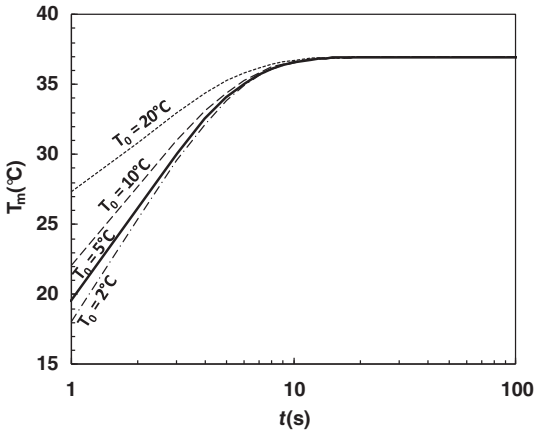

Figure 8. Time evolution of the polymer blend average temperature (T_m) referring to the configuration depicted in Figure 3(a). Four different initial temperatures (T_0) of the polymer blend are considered.

conditions, the final system is really a gel as G' and G'' are, substantially pulsation independent and G' is about one order of magnitude higher than G'' in the whole pulsation range studied.

Simulation Results

To perform model simulations, we set temperature independent density ($\rho_s = 1100$ kg m^{-3}) and thermal conductivity ($k = 0.54$ W m^{-1} k^{-1}) of the polymer blend according to Ref. 51. Figure 8, showing the time evolution of the polymer blend average temperature (T_m) for the setup depicted in Figure 3(a), tells us that heating is very fast whatever the initial temperature of the polymer blend system T_0. Indeed, heating comes to completion in about 10 s, this corresponding to an average heating speed of about 3.2 °C s^{-1}, that is, one order of magnitude higher than the highest one considered in Figures 5 and 6.

This evidence is underlined also by Figure 9 reporting the time evolution of the temperature profile inside the polymer blend and

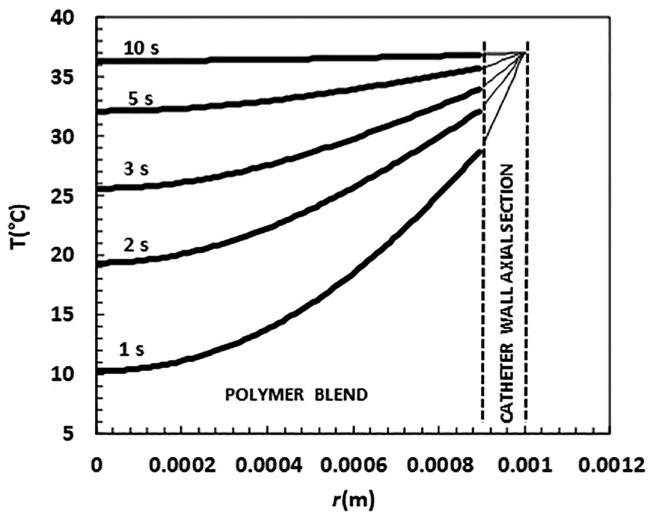

Figure 9. Time evolution of the temperature profile inside the polymer blend and the catheter wall referring to the configuration depicted in Figure 3(a) for an initial polymer blend temperature of 5 °C.

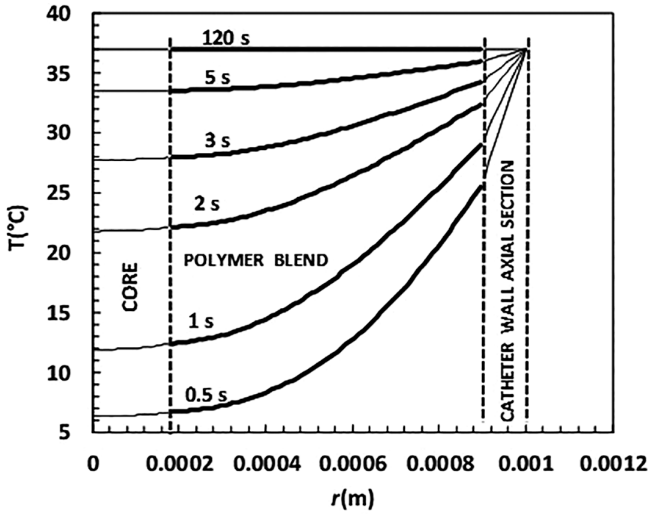

Figure 10. Time evolution of the temperature profile inside the polymer blend and the catheter wall referring to the configuration depicted in Figure 3(c) for an initial polymer blend temperature of 5 °C.

the catheter wall for the setup shown in Figure 3(a). The temperature profile occurring after 10 s is very close to the flat one (thermal equilibrium).

Similar results can be found also for the other configurations studied as witnessed by Figure 10, referring to the configuration depicted in Figure 3(c). Interestingly, Figure 11 shows that the time evolution of T_m is very similar for the configurations depicted in Figure 3(a,c,d), while a small difference occurs for the setup of Figure 3(b). This translates into similar heating speeds for configurations A, C, and D (about 3.2 °C s^{-1}) and a smaller one for case B (≈1 °C s^{-1}). Looking back to Figure 5, we can safely suppose that for these heating speeds, gelation occurs near 37 °C.

Moreover, the inspection of Figure 6 let us suppose that all these gels should be characterized by an initial value of the elastic modulus G' of, approximately, 900 Pa, that is, about one sixth of the

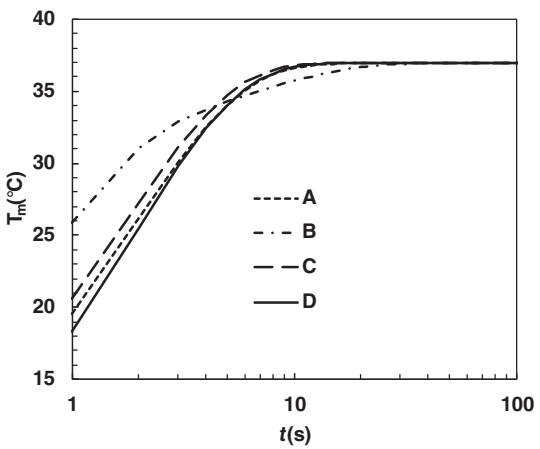

Figure 11. Time evolution of the polymer blend average temperature (T_m) referring to the configurations depicted in Figure 3(a–d). The initial temperature (T_0) of the polymer blend is equal to 5 °C.

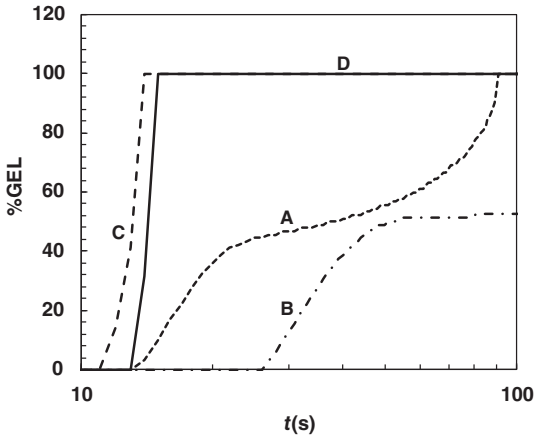

Figure 12. Kinetics of pregel formation (%GEL) referring to the configurations depicted in Figure 3(a–d). The initial temperature (T_0) of the polymer blend is equal to 5 °C.

equilibrium one (see Figures 5 and 6). According to Figure 6, the evolution toward the final G' value (i.e., that corresponding to a mature gel) takes a much longer time than that required to get catheter exit (about 120 s). This means that polymer blend solution rapidly transforms into a pregel that can flow inside the catheter as it will become a mature gel only after a very long time. Indeed, its complex viscosity (≈140 Pa s) is about one order of magnitude lower than that of the mature gel (870 Pa s). Assuming, as before stated, that gelation occur around 37 °C, Figure 12 shows the kinetics of pregel formation for the four different setup shown in Figure 3(a–d). While configurations C and D correspond to the faster kinetics, configuration A shows a slower one and only 50% of the polymer blend volume is gelled at the catheter exit for configuration B.

From a practical point of view, cases A, C, and D are very similar as they all share the condition of pregel that, once out of the catheter, is able to adhere to the coronary wall forming a layer of about 300 μm. The following exposition to divalent cations will cause the ionotropic gelation of alginate giving origin to the double layer gel. In contrast, case B seems to lead to too "liquid" system that could not have a good adhesion to the coronary wall. As case A represents just a theoretical configuration, our simulations support the validity of the proposed configurations C and D that do not significantly differ each other.

CONCLUSIONS

This work demonstrated that an aqueous polymer blend solution composed of PF127 (mass fraction 0.17) and alginate (mass fraction 0.03), flowing in a catheter for angioplasty, undergoes a very fast heating resulting in the formation of a soft pregel that can flow inside the catheter. Indeed, its transformation into a mature gel, characterized by a much higher complex viscosity, takes about 1 h, that is, a much longer time with respect to the pregel residence time inside the catheter (≈120 s). In pregel condition, the polymer blend is forced against the coronary wall where it embeds the stent strut and represents the substrate for the inotropic gelation of alginate that will give origin to a much more erosion-resistant gel. Interestingly, the improved erosion resistance of the blend system after the alginate inotropic gelation was proved by Dalmoro *et al.*[33] and by Noro[54] both of them working on a polymer blend very similar to that considered in this article. While Dalmoro worked on a simulated artery, Noro video recorded the polymer blend behavior in contact with flowing blood. In particular, Noro used a perfusion chamber where blood was induced to flow in physiological conditions through a transparent rectangular channel whose bottom part host the polymeric blend. While without alginate crosslinking the gel system was rapidly eroded, alginate crosslinking induced the disappearance of erosion (at least within the experimental time). In addition, alginate crosslinking reflected in a considerable reduction of the thrombotic effect of the polymer surface. Indeed, Noro could observe that platelets adhesion on the gel surface was considerably reduced after alginate crosslinking. Obviously, to improve our system, antithrombotic agents could be added to our formulation.

Notably, once in the proper endo-arterial location, the pluronic layer, containing the therapeutic NABD, undergoes gelation due to the body temperature. Shortly after, the exposition of the alginate layer to the appropriate amount of divalent cations, induces the gelation of the alginate. This results in the formation of a strong gel, which protects the soft pluronic layer, which has the unique function of NABD delivery material. The present approach combines the possibility to use a smart delivery material such as pluronic for endo-arterial application with the advantages of the EGP technique. For the characterization of our method, it is essential to determine the rheological behavior of the pluronic/alginate material while in the catheter to exclude early gelation, which would impede the flow into the catheter itself. Moreover, once in the arterial location the pluronic/alginate material should be in condition to form a stronger gel due to the ionotropic gelation of alginate.

Finally, our simulations indicate that the proposed configurations C and D are similar and seem to be better than configuration B, where a direct contact between the polymer blend and the metallic wire occurs. In addition, this article represents the synthesis of the work that this group has done in the last 10 years about NABD delivery to prevent traditional angioplasty drawbacks.

REFERENCES

1. Califf, R. M. *Am. Heart J.* **1995**, *130*, 680.
2. Ruygrok, P. N.; Webster, M. W.; Ardill, J. J.; Chan, C. C.; Mak, K. H.; Meredith, I. T.; Stewart, J. T.; Ormiston, J. A.; Price, S. *Catheter. Cardiovasc. Interventions*. **2003**, *59*, 165.
3. Serruys, P. W.; de Jaegere, P.; Kiemeneij, F.; Macaya, C.; Rutsch, W.; Heyndrickx, G.; Emanuelsson, H.; Marco, J.; Legrand, V.; Materne, P. *N. Engl. J. Med.* **1994**, *331*, 489.
4. Fischman, D. L.; Leon, M. B.; Baim, D. S.; Schatz, R. A.; Savage, M. P.; Penn, I.; Detre, K.; Veltri, L.; Ricci, D.; Nobuyoshi, M. *N. Engl. J. Med.* **1994**, *331*, 496.
5. Fattori, R.; Piva, T. *Lancet*. **2003**, *361*, 247.
6. Moreno, R.; Fernandez, C.; Alfonso, F.; Hernandez, R.; Perez-Vizcayno, M. J.; Escaned, J.; Sabate, M.; Banuelos, C.;

Angiolillo, D. J.; Azcona, L.; Macaya, C. *J. Am. Coll. Cardiol.* **2004**, *43*, 1964.

7. Owens, G. K.; Kumar, M. S.; Wamhoff, B. R. *Physiol. Rev.* **2004**, *83*, 767.
8. Shoji, M.; Sata, M.; Fukuda, D.; Tanaka, K.; Sato, T.; Iso, Y.; Shibata, M.; Suzuki, H.; Koba, S.; Geshi, E.; Katagiri, T. *Cardiovasc. Pathol.* **2004**, *13*, 306.
9. Bayes-Genis, A.; Campbell, J. H.; Carlson, P. J.; Holmes, D. R., Jr.; Schwartz, R. S. *Atherosclerosis*. **2002**, *163*, 89.
10. Kathuria, Y. P. *Int. J. Cardiol.* **2007**, *119*, 380.
11. Tada, T.; Byrne, R. A.; Simunovic, I.; King, L. A.; Cassese, S.; Joner, M.; Fusaro, M.; Schneider, S.; Schulz, S.; Ibrahim, T.; Ott, I.; Massberg, S.; Laugwitz, K. L.; Kastrati, A. *JACC Cardiovasc. Interv.* **2013**, *6*, 1267.
12. Iakovou, I.; Schmidt, T.; Bonizzoni, E.; Ge, L.; Sangiorgi, G. M.; Stankovic, G.; Airoldi, F.; Chieffo, A.; Montorfano, M.; Carlino, M.; Michev, I.; Corvaja, N.; Briguori, C.; Gerckens, U.; Grube, E.; Colombo, A. *JAMA*. **2005**, *293*, 2126.
13. Acharya, G.; Park, K. *Adv. Drug Deliv. Rev.* **2006**, *58*, 387.
14. Giordano, A.; Avellino, R.; Ferraro, P.; Romano, S.; Corcione, N.; Romano, M. F. *Am. J. Physiol. Heart Circ. Physiol.* **2006**, *290*, H2459.
15. Liuzzo, J. P.; Ambrose, J. A.; Coppola, J. T. *J. Invasive Cardiol.* **2005**, *17*, 497.
16. Grassi, G.; Scaggiante, B.; Dapas, B.; Farra, R.; Tonon, F.; Lamberti, G.; Barba, A.; Fiorentino, S.; Fiotti, N.; Zanconati, F.; Abrami, M.; Grassi, M. *Curr. Med. Chem.* **2013**, *20*, 3515.
17. Habib, A.; Karmali, V.; Polavarapu, R.; Akahori, H.; Cheng, Q.; Pachura, K.; Kolodgie, F. D.; Finn, A. V. *Arterioscler. Thromb. Vasc. Biol.* **2013**, *33*, 2425.
18. Navarese, E. P.; Kowalewski, M.; Kandzari, D.; Lansky, A.; Górny, B.; Kołtowski, Ł.; Waksman, R.; Berti, S.; Musumeci, G.; Limbruno, U.; van der Schaaf, R. J.; Kelm, M.; Kubica, J.; Suryapranata, H. *Open Heart.* **2014**, *1*, e000064.
19. Kobayashi, N.; Ito, Y.; Yamawaki, M.; Araki, M.; Sakai, T.; Obokata, M.; Sakamoto, Y.; Mori, S.; Tsutsumi, M.; Nauchi, M.; Honda, Y.; Tokuda, T.; Makino, K.; Shirai, S.; Hirano, K. *Int. J. Cardiovasc. Imaging.* **2018**, *34*, 1521.
20. Adriaenssens, T.; Joner, M.; Godschalk, T. C.; Malik, N.; Alfonso, F.; Xhepa, E.; De Cock, D.; Komukai, K.; Tada, T.; Cuesta, J.; Sirbu, V.; Feldman, L. J.; Neumann, F. J.; Goodall, A. H.; Heestermans, T.; Buysschaert, I.; Hlinomaz, O.; Belmans, A.; Desmet, W.; Ten Berg, J. M.; Gershlick, A. H.; Massberg, S.; Kastrati, A.; Guagliumi, G.; Byrne, R. A. *Circulation*. **2017**, *136*, 1007.
21. Byrne, R. A.; Joner, M.; Kastrati, A. *Eur. Heart J.* **2015**, *36*, 3320.
22. Jensen, L. O.; Vikman, S.; Antonsen, L.; Kosonen, P.; Niemela, M.; Christiansen, E. H.; Kervinen, K.; Erglis, A.; Harnek, J.; Kumsars, I.; Thuesen, L.; Niemela, K. *Cardiovasc. Revasc. Med.* **2017**, *18*, 577.
23. Palmerini, T.; Biondi-Zoccai, G.; Della Riva, D.; Mariani, A.; Sabate, M.; Smits, P. C.; Kaiser, C.; D'Ascenzo, F.; Frati, G.; Mancone, M.; Genereux, P.; Stone, G. W. *J. Am. Coll. Cardiol.* **2014**, *63*, 299.
24. Borovac, J. A.; D'Amario, D.; Vergallo, R.; Porto, I.; Bisignani, A.; Galli, M.; Annibali, G.; Montone, R. A.; Leone, A. M.; Niccoli, G.; Crea, F. *Eur. Heart J. Cardiovasc. Pharmacother.* **2019**, *5*, 105.
25. Grassi, G.; Dawson, P.; Kandolf, R.; Guarnieri, G.; Grassi, M. *Curr. Pharm. Biotechnol.* **2004**, *5*, 369.
26. Grassi, G.; Marini, J. C. *Ann. Med.* **1996**, *28*, 499.
27. Slepian, M. J.; Hubbell, J. A. *Adv. Drug Deliv. Rev.* **1997**, *24*, 11.
28. Davia, L.; Grassi, G.; Pontrelli, G.; Lapasin, R.; Perin, D.; Grassi, M. *Comput. Biol. Chem.* **2009**, *33*, 33.
29. West, J. L.; Hubbell, J. A. *Proc. Natl. Acad. Sci. U. S. A.* **1996**, *93*, 13188.
30. Grassi, G.; Crevatin, A.; Farra, R.; Guarnieri, G.; Pascotto, A.; Rehimers, B.; Lapasin, R.; Grassi, M. *J. Colloid Interface Sci.* **2006**, *301*, 282.
31. Grassi, G.; Farra, R.; Noro, E.; Voinovich, D.; Lapasin, R.; Dapas, B.; Alpar, O.; Zennaro, C.; Carraro, M.; Giansante, C.; Guarnieri, G.; Pascotto, A.; Rehimers, B.; Grassi, M. *J. Drug Deliv. Sci. Technol.* **2007**, *17*, 325.
32. Abrami, M.; D'Agostino, I.; Milcovich, G.; Simona Fiorentino, S.; Farra, R.; Asaro, F.; Lapasin, R.; Grassi, G.; Grassi, M. *Soft Matter*. **2014**, *10*, 729.
33. Dalmoro, A.; Barba, A. A.; Grassi, M.; Grassi, G.; Gaetano Lamberti, G. *J. Biomed. Mater. Res. B.* **2016**, *104*, 1013.
34. Grassi, G.; Farra, R.; Caliceti, P.; Grassi, M. *Am. J. Drug Deliv.* **2005**, *3*, 239.
35. Escobar-Chavez, J.; Lopez-Cervantes, M.; Naik, A.; Kalia, Y.; Quintanar-Guerrero, D.; Ganem-Quintanar, A. *J. Pharm. Pharm. Sci.* **2006**, *9*, 339.
36. Sun, J.; Tan, H. *Materials*. **2013**, *6*, 1285.
37. Tønnesen, H. H.; Karlsen, J. *Drug Dev. Ind. Pharm.* **2002**, *28*, 621.
38. Yu, G. E.; Dalton, S.; Wang, Q. G.; Attwood, D.; Price, C.; Booth, C. *J. Chem. Soc.* **1992**, *88*, 2537.
39. Doe, C.; Jang, H.-S.; Kline, S. R.; Choi, S. M. *Macromolecules*. **2009**, *42*, 2645.
40. Schmolka, I. R. *J. Am. Oil Chem. Soc.* **1977**, *54*, 110.
41. Adamo, M.; Byrne, R. A.; Baumbach, A.; Haude, M.; Windecker, S.; Valgimigli, M. *EuroIntervention*. **2016**, *12*, 1154.
42. Hinton, J.; Rawlins, J. *Medicine*. **2018**, *46*, 578.
43. Redmond, E. M.; Liu, W.; Hamm, K.; Hatch, E.; Cahill, E. P.; Morrow, D. *PLoS One*. **2018**, *9*, e84122.
44. Xu, J.; Sun, Y.; Wang, T.; Liu, G. *Mol. Cell. Biochem.* **2013**, *377*, 1.
45. Wang, J.; Liu, K.; Shen, L.; Wu, H.; Jing, H. *J. Surg. Res.* **2011**, *169*, e85.
46. Grassi, M.; Pontrelli, G.; Teresi, L.; Grassi, G.; Comel, L.; ferluga, A.; Galasso, L. *Math. Biosci. Eng.* **2009**, *6*, 493.
47. Barba, A. A.; Lamberti, G.; Rabbia, L.; Grassi, M.; Larobina, D.; Grassi, G. *Mater. Sci. Eng.* **2014**, *37*, 327.

48. Musialek, P.; Tekieli, L.; Kostkiewicz, M.; Majka, M.; Szot, W.; Walter, Z.; Zebzda, A.; Pieniazek, P.; Kadzielski, A.; Banys, P.; Olszowska, M.; Pasowicz, M.; Zmudka, K.; Tracz, W. *J. Nucl. Cardiol.* **2011**, *18*, 104.

49. Patankar, S. V. Numerical Heat Transfer and Fluid Flow; McGraw-Hill/Hemi-Hemisphere Publishing Corporation: New York, **1990**.

50. Chapra, S. C.; Canale, R. P. Numerical Methods for Engineers with Programming and Software Applications. 3rd ed.; WCB/McGraw-Hill: New York, **1998**, Chapter 11. p. 288.

51. Milocco, A. M.S. Thesis, University of Trieste, Department of Engineering and Architecture, Trieste, Italy, **2016**.

52. Barba, A. A.; d'Amore, M.; Grassi, M.; Chirico, S.; Lamberti, G.; Titomanlio, G. *J. Appl. Polym. Sci.* **2009**, *114*, 688.

53. Lapasin, R. In Polysaccharide Hydrogels: Characterization and Biomedical Application; Matricardi, P.; Alhaique, F.; Coviello, T., Eds., Pan Standford Publishing: Singapore, **2015**, Chapter 3. p. 83.

54. Noro, E. Graduate thesis, Department of Chemical, Environmental and Raw Materials Engineering, Trieste University, **2005**.